The use of XRCT to investigate highly unsaturated soil mixtures

The use of XRCT to investigate highly unsaturated soil mixtures

J.C. Smith & C.E. Augarde
School of Engineering and Computing Sciences
Durham University, Durham, UK.

C.T.S. Beckett
School of Civil and Resource Engineering
University of Western Australia, Perth, Australia.

ABSTRACT: X-Ray Computed Tomography (XRCT) is a non-destructive three-dimensional analysis technique which enables the characterisation and measurement of the internal structures of solid material samples down to sub-micron resolution. This paper describes experiences in using and developing XRCT methods and techniques to investigate unsaturated soils, specifically the microstructures of highly unsaturated soil mixtures used in earthen construction. The paper describes a study of the compressive loading behaviour of rammed earth samples which were also scanned, during which lessons were learnt regarding the use of XRCT to study soil mixtures. It is the latter which will be of most use to other researchers planning to use XRCT.

1 INTRODUCTION

X-Ray Computed Tomography (XRCT) is a non-destructive 3D imaging technique capable of imaging and analysing internal structures within solid samples to a resolution of less than one micron. The technique was first used for medical purposes followed quickly by the evaluation of its usefulness in material sciences (Reimers & Goebbels 1983). At its most basic level an XRCT machine contains three elements: the X-ray source, either a conventional X-ray tube or a synchrotron light source; a sample stage, which rotates the sample to enable a series of X-ray images to be obtained at incremental angular positions; and a detector, either a x-ray detector or a scintillator screen followed by a CCD camera (Helliwell *et al.* 2013). For a detailed description of the essentials of XRCT the reader is referred to Ketcham & Carlson (2001) for an insight into various issues, such as image artifacts and edge detection, that arise when using XRCT for quantitative analysis of materials.

1.1 *Use of XRCT in Scanning Soil Samples*

The non-destructive nature of XRCT, its ability to scan large samples to a macro-pore resolution, and the opportunity to combine results with other classic or non-destructive techniques, such as scanning electron microscopy, has made it an ideal technique for the investigation of soil and rock samples (Taina *et al.* 2008). Over the past ten years technological improvements to XRCT have seen the increasing use of the technique in the fields of soil science (Helliwell *et al.* 2013) and engineering geology (Jacobs & Cnudde 2009) although the use of XRCT in unsaturated soil research has been limited by the spatial resolution limiting the visualisation of separate particles and associated voids (Oda *et al.* 2004). However, in the last few years, XRCT has been applied to the observation of local deformation processes in sand (Hall *et al.* 2010), the mesopore size distribution of cement stabilised soils (Hall *et al.* 2013), and structural changes of unsaturated soil under loading (Beckett *et al.* 2013).

1.2 *Geotechnical research in Earthen Construction*

The soil samples used throughout this investigation were manufactured unsaturated soil mixtures used in Earthen Construction (EC). In recent years research interest has increased into the fundamental behaviour of EC materials (Beckett 2011) and suction has been shown to be a source of strength in unstabilised Rammed Earth (RE) (Jaquin *et al.* 2009). RE contains a range of particles sizes from clay to gravel, is compacted at optimum water content (w_{opt}) before being left to equilibrate to the ambient conditions and reach maximum compressive strength (Smith & Augarde 2013b). Since a considerable element of RE's strength originates from suction and RE is constructed

from a low water content manufactured soil mixture, it is therefore sensible to approach the understanding of RE fundamental material behaviour from an unsaturated soil perspective. This paper discusses the use of XRCT to monitor macrostructural changes in RE specimens of different soil texture under unconfined compression. Results are reported and implications and improvements resulting from the experience gained described.

2 DEVELOPMENT OF XRCT SCANNING METHODS

Macrostructural changes in RE materials under loading were investigated by Beckett *et al.* (2013). In that work, specimens were uniaxially loaded to either 25 or 85% of their predetermined failure load prior to scanning. This work expands on that study by investigating macrostructural changes in specimens progressively loaded to failure, not possible in the work of Beckett *et al.* (2013) due to the need to transport specimens between loading and scanning sites.

A SkyScan1174 compact micro-CT scanner (SS1174), on loan from the UK EPSRC, was used to investigate the compressive loading behaviour of RE specimens. This table-top 50kV XRCT scanner is capable of resolution down to 6μm and used a SkyScan Material Testing Stage (SSMTS) capable of applying compressive loads up to 200N. This limit restricted the size of sample that could be sheared and therefore unconfined compression (UC) tests were performed on 12mm diameter samples of RE using the SSMTS and XRCT scans performed on the samples up to and at failure. In addition to this, UC tests were performed on 27.6mm diameter samples using a Lloyd LR5K Plus Testing Machine (LR5K), capable of applying compressive loads up to 5kN. The 27.6mm diameter samples were successively scanned under unloaded, prior-to and post failure loading states, using the SkyScan1174 compact micro-CT scanner (SS1174). All scans in the SS1174 were performed at a 30.8μm resolution, using the maximum power settings of 50kV, 800μA, a 0.75mm Aluminium filter and an exposure of 7500μs. By investigating the compressive loading behaviour of the RE it was hoped that observations could be drawn regarding the development of cracks as the material failed. It was also useful to gain experience of scanning, post-processing, thresholding and analysis of images of unsaturated soils, containing a range of particles sizes from clay to gravel.

2.1 *Materials and Sample Manufacture*

Four different RE mixes were investigated each containing different proportions of gravel, sand and silty-clay. In this paper the soil mixtures are described using the Soil Mixture Classification (SMC) proposed by Smith & Augarde (2013a) whereby the soil mixture is described by its geotechnical constituents (silty-clay:sand:gravel) and the difference between the designed and manufactured proportions. The RE mixes were all manufactured in the laboratory by combining appropriate amounts of Birtley clay, sharp sand and pea gravel. The Birtley clay (1:1 kaolinitic clay-to-silt ratio by mass, LL 58.8%, PL 25.7%) was oven dried at 105°C before being pulverised and passed through a 2.36mm sieve. Both the sharp sand and the pea gravel were also oven dried at 105°C and then passed through 2mm and 10mm sieves respectively. The four soil mixes used are given in Table 1, where * denotes the combined silt and clay fractions. Dry density (ρ_d) and w_{opt} values given in Table 1 were obtained via the Vibrating Hammer Test, suggested by Smith & Augarde (2013b) to produce the closest match to compaction regimes used during construction. For all four RE mixes, five 27.6mm and five 12mm diameter samples were manufactured. Prior to the manufacture the soil mixtures were sieved to 5mm, for the 27.6mm samples, and 2mm for the 12mm samples to prevent the larger particles interfering with the compaction and loading behaviour. The appropriate amount of water was added to each mixture to reach w_{opt} and the mixture left to equilibrate overnight. The correct mass of soil mixture was then added to the 27.6mm or 12mm mould, to ensure the sample would be at its target ρ_d, and compressed to a height of 25mm and 20mm respectively. Each sample was left to dry, in a temperature monitored room at 22°C ±2°C, before the sample masses were recorded. Three samples from each batch of five manufactured samples, those closest to the batch mean dry mass, were then selected for testing. Suction was not explicitly measured but values were expected to be in the order of 20MPa to 40MPa (Jaquin *et al.* 2008).

Table 1: The target ρ_d and w_{opt} values for all four RE mixes.

RE Mix	**Optimum Water Content** (%)	**Dry Density** (gcm^{-3})
20*:70:10[1.8]	9.15	2.15
30*:60:10[0.6]	9.76	2.10
30*:50:20[0.8]	9.62	2.05
40*:50:10[2.3]	10.53	2.01

2.2 *Experimentation*

The experimental programme was split into three distinct sections: the scanning of 27.6mm samples loaded using the LR5K referred to hereafter as Lloyd Compressed Samples (LCSs); the scanning of 12mm diameter samples loaded using the SSMTS referred to hereafter as Skyscan Compressed Samples (SCSs); and the analysis of all XRCT scan data using MATLAB and ImageJ (Schneider *et al.* 2012).

2.2.1 *LCS*

The three selected samples from each batch were first scanned using the SS1174 XRCT scanner. Each scan

Table 2: The NRecon settings for all XRCT scans performed on LCSs and SCSs.

Setting	Value
Smoothing	1
Misalignment Compensation	Auto
Ring Artifacts Reduction	15
Beam-hardening correction	25%
Histogram Values	Auto
Number of Slices	1000

took approximately 100 minutes using a rotation step of 1° and an averaging of 2 frames. This enabled multiple scans to be run within a working day whilst ensuring the scan quality was high enough for reconstruction to take place. The scan obtained was taken as the pre-loading scan. A UC test was then performed using the LR5K, at a rate of 0.1mm/minute, until failure was observed by evidence of a load peak. Compression was then immediately stopped and the load released. During compression the load applied and displacement of the loading plate was logged using "Triax" software. The sample, with great care, was then placed inside the SS1174 and re-scanned. This was taken as the post-loading scan.

2.2.2 *SCS*

The three selected samples from each batch were in turn placed inside the SkyScan load cell installed within the SS1174. A pre-loading scan was performed taking approximately 25 minutes using a rotation step of 2°. A UC test was then performed using the SSMTS, at a rate of 0.01mm/minute, to failure. At 25N intervals, and immediately after failure, the SSMTS was paused to enable fast scans to be performed on the SS1174, taking 10 minutes using a rotation step of 5°. The load was then released and a post-loading scan performed using the pre-scan settings. The fast scans were required due to the poor load control from the SSMTS during scans. Critically, it was found that the load applied could drop during a scan, up to 25N over 30 minutes, and so to ensure a constant load was maintained during scanning the time taken had to be limited to 10 minutes. In turn, the pre-loading and post-loading time was chosen to ensure two samples could be scanned and tested within a single working day.

2.2.3 *Post Processing & Analysis*

All XRCT scans performed on both LCSs and SCSs were reconstructed using SkyScan NRecon software with the settings shown in Table 2. The 840 slices, across the depth of the sample, used in reconstruction ensured the vertical resolution matched the 30.8µm from the scans and no detail in the vertical plane was lost during post-analysis. The scans were then batch processed, via MATLAB, using custom-written ImageJ macros to calculate, for every slice, the percentage of cracks by area within the sample.

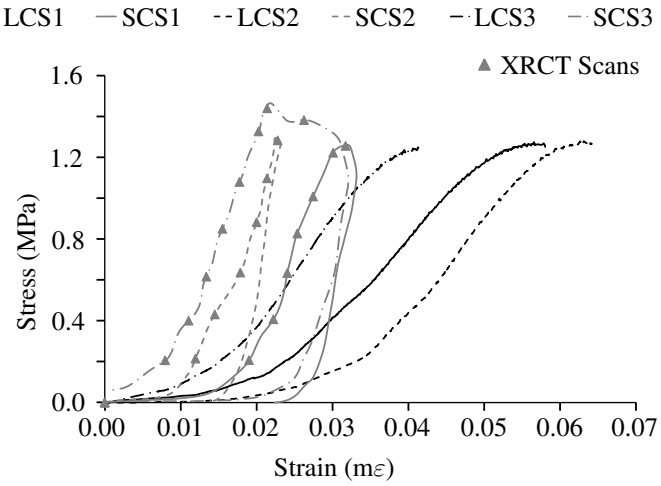

Figure 1: Vertical axis stress-strain results, with XRCT scans indicated, for all six 40*:50:10[2.3] samples.

Table 3: The failure stress and strain values for all four RE mixes. Entries in bracketed italics were deemed anomalous.

RE Mix	Failure Stress (MPa)		
	Sample 1	Sample 2	Sample 3
20*:70:10[1.8]LCS	*(0.62)*	0.80	0.75
30*:60:10[0.6]LCS	1.11	1.17	*(0.75)*
30*:50:20[0.8]LCS	0.73	0.71	*(0.95)*
40*:50:10[2.3]LCS	1.27	1.28	1.25
20*:70:10[1.8]SCS	*(0.65)*	1.19	1.21
30*:60:10[0.6]SCS	1.60	1.52	1.54
30*:50:20[0.8]SCS	1.75	1.64	*(1.20)*
40*:50:10[2.3]SCS	1.26	1.29	*(1.46)*

2.3 *Results & Analysis*

2.3.1 *Stress strain results*

Figure 1 shows the vertical axis stress - strain results obtained for both the 40*:50:10[2.3] LCSs and SCSs. Table 3 shows the failure stress values obtained for all LCSs and SCSs. Six failure stress values were found to be clear outliers, taken as anomalous and the samples were disregarded for the remainder of the analysis. The two sample sizes, 12mm and 27.6mm, produced different vertical axis stress-strain plots and resulted in different compressive failure stresses for the same RE mixes. This difference in failure stresses was also identified by Ciancio & Gibbings (2012), who found the shape and size of cement-stabilised RE affected the material strength. This is likely to have been due to the different load rates applied and the sieving of different particle sizes, $>$ 2mm and $>$ 5mm, out of the soil mixture prior to manufacture. Figure 2 shows an increasing discrepancy between the failure stresses of the two sizes of sample tested as the ratio between the gravel and silt/clay fractions decrease. This suggests that for the mixes where clay/silt fraction dominates the gravel fraction, i.e. 40*:50:10[2.3], the removing of the largest particles has minimal effect on the final failure load whilst the mixes where the two fractions are more similarly proportioned, i.e. 30*:50:20[0.8], the removing of the particles dramatically changes the failure stress. This is as expected, as removal of particles from these mixes constitutes the greatest change in soil texture.

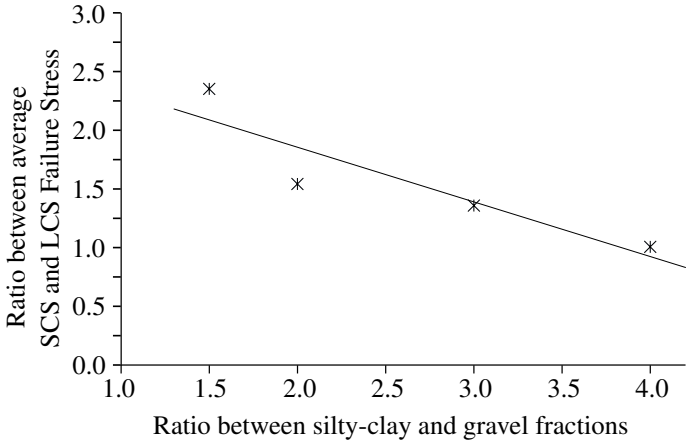

Figure 2: The ratio of silty-clay:gravel plotted against the ratio of failure stress for SCS:LCS.

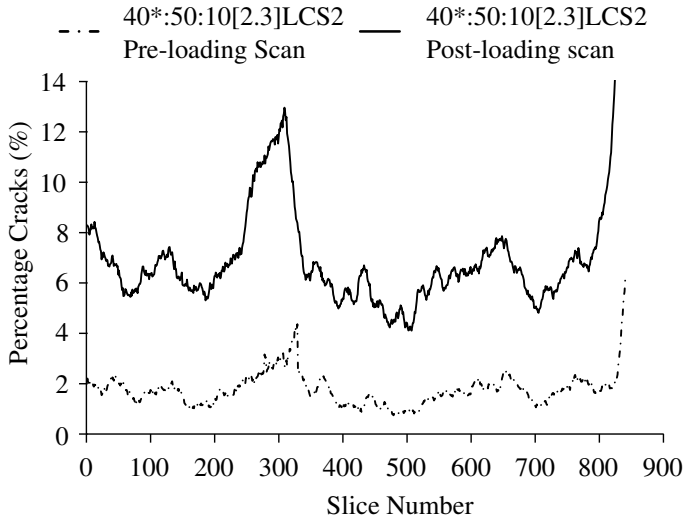

Figure 3: The area of cracks for each slice of 40*:50:10[2.3] LCS2. Slice Number relates to depth below top surface of the sample, with slices spaced at 29.8μm.

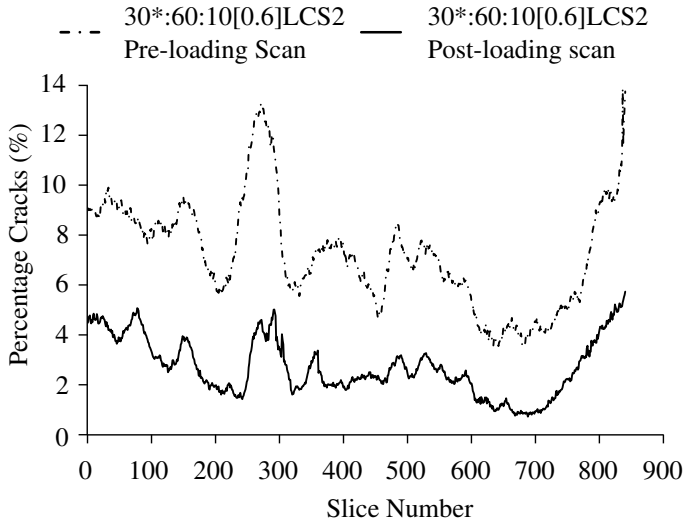

Figure 4: The area of cracks for each slice of 30*:60:10[0.6] LCS2. Slice Number relates to depth below top surface of the sample, with slices spaced at 29.8μm.

Table 4: A summary of all XRCT analysis for LCSs indicating the change in percentage of cracks following compressive loading.

RE Mix	Change in % cracks following loading
20*:70:10[1.8]LCS2	increase
20*:70:10[1.8]LCS3	increase
30*:60:10[0.6]LCS1	decrease
30*:60:10[0.6]LCS2	increase
30*:50:20[0.8]LCS1	decrease
30*:50:20[0.8]LCS2	decrease
40*:50:10[2.3]LCS1	increase
40*:50:10[2.3]LCS2	increase
40*:50:10[2.3]LCS3	increase

2.3.2 *LCS XRCT scan results*

Only the LCS results are presented and discussed here due to the unsuccessful analysis of the SCS XRCT scans, discussed in Section 2.3.3. All the LCS samples were successfully scanned and analysed, although the results for the six anomalous failure stress results were discounted, as discussed in Section 2.3.1.

When considering the 40*:50:10[2.3] and 20*:70:10[1.8] LCS crack percentages a clear result can be observed. As shown by Figure 3, the area of cracks in each layer significantly increases after the sample has been loaded to failure. However, as shown by Figure 4 and Table 4, not all the RE mixes behave in the same way - with three samples showing the percentage of cracks reducing in all slices. On further examination of the percentage crack plots it is clear that the shape of both the pre- and post- loading crack percentage lines are very similar for all samples, whether showing an increase or decrease. Two possible explanations exist for these similarities in shape, the first associated with the material behaviour of the samples and the second linked to the XRCT scanning and analysis process. The first and expected outcome, supported by two-thirds of the results, was that since the sample has reached failure the size and quantity of cracks would increase after loading. From a material behaviour perspective cracks will grow throughout the sample as the material fails resulting in an increase in crack percentage across all slices. This however cannot explain the clear decrease in cracks observed for the 30*:60:10[0.6]LCS1, 30*:50:20[0.8]LCS1 and 30*:50:20[0.8]LCS2 samples and a second explanation needs considering.

From an XRCT scanning perspective it is possible that the change in crack percentage is simply due to differences in the brightness of the pre-loading and post-loading scans causing the crack threshold value to increase. During the initial writing of the ImageJ analysis macros a preliminary investigation was performed into the appropriate threshold values for cracks. 48 local histograms were obtained, across a range of different samples, for areas manually identified as cracks and a single threshold value determined for full analysis of all samples. The problem with this method was its assumption that the grey-scale his-

tograms produced by the SS1174, in which pixel intensity values relate to densities within the sample, was the same across all the scans performed. Following post-processing and analysis it became clear this was not the case. During the scanning process, where the x-ray image is converted to a 255 incremented grey scale image, the SS1174 chose the density-grey scale correlation for every scan to provide maximum clarity related to the most dense point within the sample. This meant that for every sample scan performed, either two different samples or the same sample before and after loading, the correct threshold for cracks would have been slightly different and, since a universal threshold value was used, crack percentages obtained were not perfectly correct. Larger, and more expensive, XRCT scanners are capable of also presenting the "true image", not scaled to provide the best clarity for any individual scan, however this was not possible with the SS1174. It would therefore seem sensible, when this true image is not available, to include two reference points, using two materials of known density, which set the maximum and minimum values within the density spectrum and therefore the density-greyness correlation.

2.3.3 *SCS XRCT scan results*

Following visual inspection the quality of the SCS SS1174 scans appeared sufficient, since the cracks could be manually identified. However, the thresholds applied and analysis techniques used were unable to identify the required features with sufficient autonomy for the analysis to be batch processed and run on a total of $>10^5$ slices. This was due to poor reconstruction quality because of a lack of initial scan images caused by the increased angle of rotation between scans. Therefore all the SCS reconstructions were not of sufficient quality to analyse, due to the use of a more rapid scan setting, and no numerical data is presented here. Despite this however, the lack of useful XRCT scan results from the SCS raises a number of clear observations and lessons of note.

Firstly, using visual inspection to assess the quality of a scan can lead to problems when writing analysis techniques to identify objects or areas of interest. It is suggested that preliminary scans are not only checked visually but, where possible, are analysed using computational post-processing software to ensure the required quality of results are obtainable. Secondly, speeding up the scanning process to increase the samples scanned during a day is ultimately unproductive if the resulting scans are not of sufficient quality. The pre and post loading SCS scans, where no load was applied to sample, were not constrained by any time factors other than a desire to scan more samples in a given time, and decreasing the scan time resulted in all the scans simply producing some indicative 3D models rather than scans capable of producing quantitative data for analysis. Had the first lesson discussed been implemented, where preliminary scans were analysed rather than only visually inspected, the same scan settings used in the LCS scans, taking approximately an hour, could have been implemented and the resulting scans would have been suitable for the post-processing analysis. It is therefore suggested that scan quality should be the driving factor and not time, which can be tempting when there is limited time available on a given XRCT scanner.

Caution must be also be taken when reducing scan times or reconstruction times through the increase of rotation angle or reduction in number of slices. The resolution of the final reconstruction is not only dependant on the zoom applied by the XRCT scanner but also on the number of slices in the reconstruction, affecting the resolution in the vertical plane, and the angle of rotation of the sample, affecting the true resolution in the horizontal plane. For both the LCS and SCS scans the use of 840 slices, across the depth of the sample, ensured the scan resolution of 30.8μm was maintained during reconstruction. The 5^o, 2^o & 1^o angles of rotation of the samples also ensured the 30.8μm resolution was maintained in the plane of rotation, with points moving with each rotation of the sample relative to the x-ray detector a maximum of 22.8μm on the very edge of each sample. It might be suggested that the 2^o & 1^o angles of rotation were unnecessary, since the 5^o rotation was acceptable, however by reducing the rotation angle, and in turn increasing the number of images, the quality of the sample reconstruction was improved. It is therefore important to note that reducing the number of slices, or increasing the angle of rotation, can be very attractive when trying to reduce the time required but this must be done with great care. The impact on the scan quality and the true resolution of the resulting reconstruction must be calculated and it cannot be assumed that since the XRCT scanner was set to a specific resolution that this will still hold once the 3D reconstruction of the sample is complete.

2.4 *Key Observations*

The results obtained and time spent using the SS1174 prompts a number of key observations:

Firstly, the use of different sample sizes, with different maximum particle size, can change the mechanical behaviour of the earthen construction mix. It is therefore important to consider the impact of sieving samples, to aid compaction or XRCT scan quality, for the particular soil mixture being investigated. The effect of this, as discussed in Section 2.3.1, can be most clearly seen in mixes where the soil silty-clay and gravel fractions are more similarly proportioned.

Secondly, it is very important to not rush the scanning process, no matter the conditions of the sample, to ensure the quality of the scan is suitable for the required analysis. As became evident following analysis of the SCS XRCT scans speeding up the scan process, to ensure the load applied did not reduce, caused

the quality of the scans to be of insufficient quality to analyse and it would have better not to have scanned the samples during loading at all, since machine time would not have been wasted on obtaining poor quality data.

Thirdly, when trying to compare two scans, either two samples from the same batch or the same sample before and after loading, it is crucial that the relationship between density and intensity of individual pixels is fixed to ensure the scans are compared under the same conditions. When using the SS1174 it was impossible to fix this density conversion, as the machine automatically scaled the outputted grey-scale image relative to the most dense object within the scan. In this case it is suggested that two reference objects, of differing known densities, are placed in all scans performed to enable the adjustment of the scans during postprocessing to ensure all the scans can be compared under the same conditions.

3 FUTURE WORK

The second stage of the investigation into the structure of highly unsaturated earthen construction materials using XRCT began with the installation of an XRadia/ZeissXRM 410 (XRM410) XRCT scanner in the Durham University School of Engineering and Computing Sciences in September 2013. Capable of resolutions down to 0.9μm and scanning samples up to 300mm in size, the XRM410 has provided considerably higher resolution and contrast images of the RE samples. Initial tests and experiments are being performed as this paper goes to press and will be reported at the conference.

4 CONCLUSIONS

Three key points emerged from this investigation. Firstly, desktop scanners, such as the SS1174, are not best suited for EC samples as higher quality scans are required for quantitative analysis and can be easily obtained using a more powerful scanner such as the XRM410. Secondly, the sieving of EC mixes to remove large particles, and ensure reliable results when testing small diameter samples, can considerably effect failure stresses. For samples in which the gravel and clay/silt fractions are more similarly proportioned this effect is most pronounced. Finally, when trying to compare samples scanned at different times, or run batch analyses on multiple samples, the scaling of the grey-scale image relative to density must be fixed for all scans. It is suggested this be achieved through the insertion of two reference materials into all scans or by obtaining the true adsorption image, available with more advanced XRCT scanners.

REFERENCES

Beckett, C. (2011). The role of material structure in compacted earthen building materials: implications for design and construction. *PhD Thesis, Durham University*.

Beckett, C., M. Hall, & C. Augarde (2013). Macrostructural changes in compacted earthen construction materials under loading. *Acta Geotechnica 8*(4), 423–438.

Ciancio, D. & J. Gibbings (2012). Experimental investigation on the compressive strength of cored and molded cement-stabilized rammed earth samples. *Construction and Building Materials 28*, 294–304.

Hall, M., S. Mooney, C. Sturrock, P. Matelloni, & S. Rigby (2013). An approach to characterisation of multi-scale pore geometry and correlation with moisture storage and transport coefficients in cement-stabilised soils. *Acta Geotechnica 8*(1), 67–79.

Hall, S., M. Bornert, J. Desrues, Y. Pannier, N. Lenoir, G. Viggiani, & P. Besuelle (2010). Discrete and continuum analysis of localised deformation in sand using x-ray μct and volumetric digital image correlation. *Géotechnique 60*(5), 315–322.

Helliwell, J., C. Sturrock, K. Grayling, S. Tracy, R. Flavel, I. Young, W. Whalley, & S. Mooney (2013). Applications of x-ray computed tomography for examining biophysical interactions and structural development in soil systems: a review. *European Journal of Soil Science 64*(3), 279–297.

Jacobs, P. & V. Cnudde (2009). 'Applications of x-ray computed tomography in engineering geology' or 'looking inside rocks...'. *Engineering Geology 103*, 67–68.

Jaquin, P., C. Augarde, D. Gallipoli, & D. Toll (2009). The strength of unstabilised rammed earth materials. *Géotechnique 59*(5), 487–490.

Jaquin, P., C. Augarde, & L. Legrand (2008). Unsaturated characteristics of rammed earth. *Unsaturated soils: advances in geo-engineering: proceedings of the 1st European Conference on Unsaturated Soils*, 417–422.

Ketcham, R. & W. Carlson (2001). Acquisition, optimization and interpretation of x-ray computed tomographic imagery: applications to the geosciences. *Computers & Geosciences 27*(4), 381–400.

Oda, M., T. Takemura, & M. Takahashi (2004). Microstructure in shear band observed by microfocus x-ray computed tomography. *Géotechnique 54*, 539–542.

Reimers, P. & J. Goebbels (1983)). New possibilities of non-destructive evaluation by x-ray computed tomography. *Materials Evaluation 41*, 732737.

Schneider, C., W. Rasband, & K. Eliceiri (2012). NIH Image to ImageJ: 25 years of image analysis. *Nat Methods 9*(7), 671–675.

Smith, J. & C. Augarde (2013a). A new classification for soil mixtures with application to earthen construction. *ECS Technical Report ECS-TR 2013/04, Published 20.09.2013*.

Smith, J. & C. Augarde (2013b). Optimum water content tests for earthen construction materials. *Proceedings of the ICE - Construction Materials To appear, available online: 02 May 2013*.

Taina, I., R. Heck, & T. Elliot (2008). Application of x-ray computed tomography to soil science: A literature review. *Canadian Journal of Soil Science 88*(1), 1–19.